Nuclear Materials and Energy 20 (2019) 100599

Contents lists available at ScienceDirect

Nuclear Materials and Energy

journal homepage: www.elsevier.com/locate/nme

# Using EDGE2D-EIRENE to simulate the effect of impurity seeding and fueling on the upstream electron separatrix temperature

J. Simpson[a,b,c,*], D. Moulton[a], C. Giroud[a], M. Groth[b], G. Corrigan[a], JET Contributors[1]

[a] EUROfusion Consortium, JET, Abingdon, Oxfordshire OX14 3DB, United Kingdom
[b] Aalto University, 02150 Espoo, Finland
[c] CCFE, Culham Science Centre, Abingdon, OX14 3DB, United Kingdom

ARTICLE INFO

*Keywords:*
Separatrix temperature
EDGE2D-EIRENE

ABSTRACT

The edge fluid code EDGE2D-EIRENE was used to compare the calculated low field side mid-plane separatrix temperature ($T_{eu,\ sep}$) in the presence of seeding impurities with the two point model. The value of $T_{eu,\ sep}$ and scalings of $T_{eu,\ sep}$ with the power crossing the separatrix ($P_{sep}$) are studied. Two scalings of $T_{eu,\ sep}$ with $P_{sep}$ can be derived from two point model; (1) $T_{eu,sep} \propto P_{sep}^{\frac{2}{7}}$ which assumes that the power decay length $\lambda_q$ is constant and; (2) $T_{eu,sep} \propto P_{sep}^{\frac{4}{9}}$ which accounts for the $\lambda_q$ dependence on $P_{sep}$ and the presence of prescribed diffusive radial transport. A linear scaling between $T_{eu,\ sep}$ and $P_{sep}$ is observed in the EDGE2D simulations, although the $T_{eu,sep} \propto P_{sep}^{\frac{4}{9}}$ scaling captures the variation in $T_{eu,\ sep}$ (in the simulations) for all but highly seeded simulations. This linear dependence (between $T_{eu,\ sep}$ and $P_{sep}$) is due to a stronger than linear dependence on the parallel heat flux entering the divertor ($q_{\parallel,\ u,\ sep}$) on $P_{sep}$ (for a doubling of $P_{sep}$ a factor six variation in $q_{\parallel,\ u,\ sep}$ is observed). $P_{sep}$ is reduced by a factor of two due to the varying impurity radiation inside the separatrix. However, $q_{\parallel,\ u,\ sep}$ reduces more than a factor two because (i) impurity radiation preferentially removes heat flux above the *x*-point and near the separatrix and (ii) the variation in $\lambda_q$ with $P_{sep}$ due to increasing radial diffusive heat flux (Eq. (5.77) Stangeby 2000). The largely varying $q_{\parallel,\ u,\ sep}$, interestingly, is successfully captured by the power decay length ($\lambda_{q,\ Eich}$) calculated by fitting to the target heat flux density. Accounting for the $q_{\parallel,\ u,\ sep}$ variation by using $\lambda_{q,\ Eich}$ and $P_{sep}$ (both experimentally measurable quantities), an agreement between the two point model equation and the predicted $T_{eu,\ sep}$ from EDGE2D-EIRENE was obtained. A variation of $T_{eu,\ sep}$ from approximately 60 eV to 120 eV, for electron separatrix density range of $2 - 3 \times 10^{19}$ m$^{-3}$, was observed. This separatrix temperature variation from EDGE2D is in contrast to a routinely assumed separatrix temperature of 100 eV used for pedestal stability analysis at JET.

## 1. Introduction

The separatrix temperature is required as an input for several models of the tokamak edge. For example, the heuristic power decay length ($\lambda_q$) model in reference [1], H-mode density limit studies in reference [2] and pedestal stability analysis [3]. In these models the fundamental equation used to approximate the separatrix temperature is the two point model equation [4]:

$$T_{eu,sep} = \left(\frac{7 q_{\parallel,u,sep} L}{2\kappa}\right)^{\frac{2}{7}} \quad (1)$$

Here, $T_{eu,\ sep}$ is the upstream electron temperature (eV), which is taken at the low field side (LFS) midplane separatrix, $q_{\parallel,\ u,\ sep}$ is the total heat flux (assuming that the ion heat flux is small) at the entrance to the divertor on the LFS at the separatrix (Wm$^{-2}$), $L$ is the connection length (m) and $\kappa = 2000$ (Wm$^{-1}$eV$^{-\frac{7}{2}}$).

Practically the models referenced above use the following equation to approximate $T_{eu,\ sep}$ because it contains experimentally measurable variables unlike $q_{\parallel,\ u,\ sep}$. To derive this equation the approximation $q_{\parallel,\ u,sep} \sim (P_{sep}/2)/A_q$ is applied to Eq. (1) to yield [4]:

$$T_{eu,sep} = \left(\frac{7((P_{sep}/2)/A_q) L}{2\kappa}\right)^{\frac{2}{7}} \quad (2)$$

Here, $P_{sep}$ is power crossing the last closed flux surface from the

* Corresponding author at: CCFE, UKAEA, Abingdon, Oxford OX14 3GY, United Kingdom.
*E-mail address:* james.simpson@ukaea.uk (J. Simpson).
[1] See the author list of "X. Litaudon et al. 2017 Nucl. Fusion 57 102001".

https://doi.org/10.1016/j.nme.2019.02.002
Received 14 August 2018; Received in revised form 14 January 2019; Accepted 1 February 2019
Available online 05 June 2019

**Table 1**
The markers used to represent the parameters in the simulation scan are shown in this table. Blue markers are neon seeding, green markers are nitrogen seeding and black are unseeded. The size of the symbol represents an increase in separatrix electron density ($n_{e,\ sep}$). The different types of the symbol are to represent different impurity radiation powers. The open symbols represent simulations which have had the impurity radiation in the main SOL (above the *x*-point) removed from the total radiation of the simulation. The colour, shape and size of the open symbol retain the same meaning as the closed symbols.

| | | | | Impurity radiation ($P_{rad}$) | | | | |
|---|---|---|---|---|---|---|---|---|
| | | 0 MW | 2 MW Neon | 2MW Nitrogen | 4 MW Neon | 4 MW Nitrogen | 6 MW Neon | 6MW Nitrogen |
| $n_{e,sep}$ | $2x10^{19}\ m^{-3}$ | ● | ▲ △ | ▲ △ | ■ □ | ■ □ | ★ ☆ | ★ ☆ |
| | $2.5x10^{19}\ m^{-3}$ | ● | ▲ | ▲ | ■ | ■ | ★ | ★ |
| | $3x10^{19}\ m^{-3}$ | ● | ▲ △ | ▲ △ | ■ □ | ■ □ | | |

confined plasma (W) and

$$A_q = 2\pi R\lambda_q\left(\frac{B_\vartheta}{B}\right) \quad (3)$$

where $A_q$ is the area perpendicular to a (toroidally extended) flux tube of width $\lambda_q$ ($m$) that $P_{sep}$ falls over, $\lambda_q$ is the power decay width at the upstream position, $R$ ($m$) is the radius at the upstream position, and $(\frac{B_\vartheta}{B})$ is the ratio of the poloidal magnetic field to the total magnetic field at the upstream location. Note that Eq. (2) assumes no power loss between the *x*-point and the upstream position (low field side mid-plane separatrix).

From Eq. (2) two scalings between the $T_{eu,\ sep}$ and $P_{sep}$ can be derived; (1) $T_{eu,sep} \propto P_{sep}^{\frac{2}{7}}$ which is derived assuming that $P_{sep}$ is only significantly varying parameter and, (2) $T_{eu,sep} \propto P_{sep}^{\frac{4}{9}}$ which is derived assuming that $\lambda_q$ in Eq. (2) can be calculated as a competition between conductive parallel heat transport and prescribed radial diffusive heat transport, in which case $\lambda_q \propto P_{sep}^{-\frac{5}{9}}$ (Equation (5.77) from reference [4]).

$T_{eu,\ sep}$ is a boundary condition for pedestal stability analysis codes [5]. The weak power dependence of $P_{sep}$ from the scaling $T_{eu,sep} \propto P_{sep}^{\frac{2}{7}}$ is often used to justify the assumption that the variation in $T_{eu,\ sep}$ can be neglected [5]. So, a value of 100 eV is often assumed as the $T_{eu,\ sep}$ boundary condition for pedestal stability analysis for the JET, independent of the specifics of a particular JET discharge.

Work presented in references [6,7] considered the effect of nitrogen seeding using EDGE2D-EIRENE. However, the authors focussed on the effect on the divertor and comparison to experiment rather than the upstream effects examined in this paper.

In this work the applicability of Eq. (2) and the variation in $T_{eu,\ sep}$ was assessed using the edge fluid neutral code EDGE2D-EIRENE [8–10]. Simulations were conducted with varying neon and nitrogen seeding radiation and a range of electron separatrix densities ($n_{e,\ sep}$). The effect of neon seeding on $T_{eu,\ sep}$ has not been examined previously. Impurities, either intrinsically sputtered or injected deliberately e.g. for heat load control [11], introduce losses between the upstream and downstream locations. The validity of Eq. (2) due to this assumption has been examined in this work in order to provide guidance on its continued application. Furthermore, the legitimacy of the $T_{eu,sep} \propto P_{sep}^{\frac{2}{7}}$ and $T_{eu,sep} \propto P_{sep}^{\frac{4}{9}}$ scalings will be assessed within this paper.

## 2. Simulation set up

The edge fluid code EDGE2D [8] coupled to the kinetic neutral Montel-Carlo code EIRENE [9,10] was used to simulate a high confinement mode plasma in a set up as shown in reference [7] (high field side (HFS) and LFS strike points were located on the vertical target). The main fuel puff location was the same as used in reference [7]. However the impurity puff location was moved to the LFS target in the private flux region so that it was in the same location as the experimental results presented in [11].

Simulations with two different seeding impurities – neon and nitrogen - were conducted. The impurities due to seeding were controlled within the simulation such that the total impurity seeding radiation achieved was either 2, 4 or 6 MW. For each seeded impurity and radiation power, a scan in upstream $n_{e,\ sep}$ was performed where the density was set to either 2, 2.5 or 3 $\times 10^{19}$ m$^{-3}$. A total input power of 8 MW (split evenly between the ion and electron channel) was set as the core boundary condition for the heat flux into the domain. This parameter range was chosen to be representative of H-mode-like conditions for seeding scenarios [11]. The 3 $\times 10^{19}$ m$^{-3}$, 6 MW, neon and nitrogen seeded simulations are not presented here due to code convergence issues. Unseeded reference cases were also simulated for each $n_{e,\ sep}$. Beryllium was also included as a sputtered impurity from the main chamber wall in only the seeded simulations. Drifts and currents were not included within these simulations.

The radial transport in EDGE2D-EIRENE is diffusive only and prescribed. The radial particle and heat diffusion profiles were taken directly from references [12,13] for the main ions and electrons, and remained fixed throughout the presented parameter scan. Below the *x*-point the radial particle transport coefficients were set to 1 m$^2$s$^{-1}$ for the main ion and electrons. For the impurity ions it was assumed that the radial particle transport is poloidally and radially constant at 0.6 m$^2$s$^{-1}$ both above and below the *x*-point. The choice of the impurity transport coefficient is arbitrary, yet reasonable, due to having limited experimental knowledge about the radial transport of the impurity ions and aided in code convergence. The inclusion of a particle transport barrier in the radiating impurity was tested because a transport barrier was used in the main ions. At low, $n_{e,\ sep}$, $T_{eu,\ sep}$ increased up to approximately 40%. However, the impurity transport barrier was found to produce very large core $Z_{effective}$ values, which were not experimentally relevant. At the highest $n_{e,\ sep}$ within this parameter scan, the transport barrier had minimal effect on $T_{eu,\ sep}$ and $Z_{effective}$.

Details of the symbols used to represent the simulation on the proceeding figures are shown in Table 1.

## 3. Results

The purpose of this study was to compare the predicted $T_{eu,\ sep}$ from EDGE2D-EIRENE with the prediction from Eq. (2). EDGE2D-EIRENE

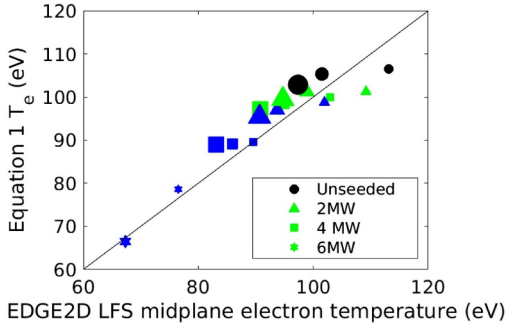


**Fig. 1.** The upstream electron temperature calculated using the two point model equation $T_{eu,sep} = (\frac{7q_{\|}L}{2\kappa})^{\frac{2}{7}}$ plotted against the EDGE2D temperature taken at the LFS midplane. The markers represent the total seeding radiation: circle – 0 MW (i.e. unseeded); triangle – 2 MW; square – 4 MW; 6-point star – 6 MW. The colour represents the seeding impurity: black – unseeded; green – nitrogen; blue – neon. Increasing size of the symbol represents increasing electron separatrix density ($n_{e,\ sep}$) where the smallest symbol is $n_{e,sep} = 2\ \times 10^{19}$ and the largest is $n_{e,sep} = 3\ \times 10^{19}\ m^{-3}$. (For interpretation of the references to colour in this figure legend, the reader is referred to the web version of this article.)

was used as a synthetic experiment; parameters $P_{sep}$, $L$ and $A_q$ were extracted from EDGE2D to calculate Eq. (2) for a comparison with $T_{eu,\ sep}$ predicted by EDGE2D-EIRENE.

### 3.1. Scaling of the upstream temperature with $\boldsymbol{q}_{\|}$ and $\boldsymbol{P}_{\boldsymbol{sep}}$

The derivation of Eq. (1) is based on the following assumptions: (1) the heat transport from the upstream to the downstream location is exclusively electron conduction (assuming it is much greater than the ion conductive heat flux) and calculated according to Spitzer–Härm [4]; (2) $T_{eu,\ sep}$ is much greater than the downstream temperature i.e. $T_{eu,sep}^{\frac{7}{2}} \gg T_{et,sep}^{\frac{7}{2}}$; (3) $\kappa$ remains constant along a field line; (4) $Lq_{\|,\ u,\ sep}$ captures the entire variation of the heat flux along the field line, i.e. $\int_0^L q_{u,\|}(s_{\|})\ ds_{\|} \sim Lq_{\|,u,sep}$.

First, it must be established whether the assumptions stated in the previous paragraph can be validated within the presented parameter scan in order to proceed with a comparison of Eq. (2). Eq. (1) was calculated using the total $q_{\|}$ at the divertor entrance at the separatrix ($q_{\|,\ u,\ sep}$), $L$ is calculated from the LFS target to the LFS midplane for all cases, and $\kappa = 2000$ ($\mathrm{Wm^{-1}eV^{-\frac{7}{2}}}$) . Fig. 1 shows an agreement between the $T_{eu,\ sep}$ measured in EDGE2D-EIRENE and the prediction from Eq. (1). Note the low density unseeded case (smallest black circle Fig. 1) is sheath limited, and when including the target temperature in Eq. (1) gives a better agreement with EDGE2D. The agreement was approximately within 20% at worst, and so a comparison with Eq. (2) was carried out.

The scaling $T_{eu,sep} \propto q_{\|,u,sep}^{\frac{2}{7}}$ (as per Eq. (1)) for this simulation set, is valid due to all other variables in Eq. (1) (except $q_{\|,\ u,\ sep}$) being constant because the equilibrium remained fixed throughout the simulation set and $\kappa^{\frac{2}{7}}$ remained approximately constant due to being a weak function of the plasma parameters. Approximately a factor six change in $q_{\|,\ u,\ sep}$ at the divertor entrance was observed (Fig. 2); hence the large variation in $q_{\|,\ u,\ sep}$ drives the two fold variation in $T_{eu,\ sep}$. Based on the observation that $T_{eu,sep} \propto q_{\|,u,sep}^{\frac{2}{7}}$ scaling is correct and $q_{\|,\ u,\ sep}$ varies by a factor six, it could be expected that $P_{sep}$ would also vary by a factor six ($q_{\|,u,sep} \propto P_{sep} \therefore T_{eu,sep} \propto P_{sep}^{\frac{2}{7}}$). However, a linear scaling between $T_{eu,\ sep}$ and $P_{sep}$ was found (Fig. 3 solid markers), thus $P_{sep}$ only varies by approximately a factor two which would not support a factor two variation in $T_{eu,\ sep}$. Hence, for the presented simulations, the scaling $T_{eu,sep} \propto P_{sep}^{\frac{2}{7}}$ (solid lines Fig. 3) is not sufficient to explain the factor two variation in $T_{eu,\ sep}$.

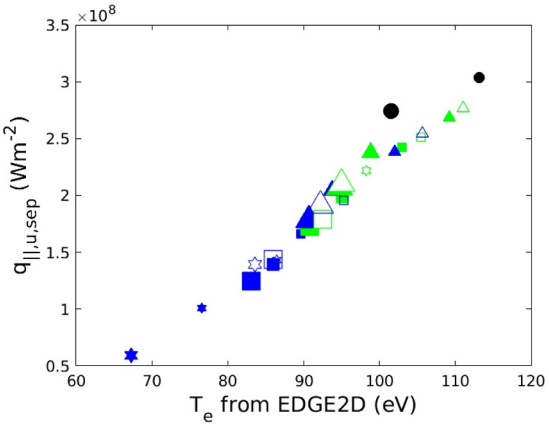


**Fig. 2.** The parallel heat flux at the separatrix at the divertor entrance plotted against the upstream LFS electron separatrix temperature from EDGE2D. The markers represent the total seeding radiation: circle – 0 MW (i.e. unseeded); triangle – 2 MW; square – 4 MW; 6-point star – 6 MW. The colour represents the seeding impurity: black – unseeded; green – nitrogen; blue – neon. Increasing size of the symbol represents increasing electron separatrix density ($\boldsymbol{n}_{\boldsymbol{e,\ sep}}$) where the smallest symbol is $\boldsymbol{n}_{\boldsymbol{e,sep}} = 2 \times 10^{19}$ and the largest is $\boldsymbol{n}_{\boldsymbol{e,sep}} = 3 \times 10^{19}\ \boldsymbol{m}^{-3}$. The open symbols represent the same plasma parameters as the filled symbols except within the simulation the impurity radiation has been removed from the scrape-off layer above the $x$-point. (For interpretation of the references to colour in this figure legend, the reader is referred to the web version of this article.)

The scaling $T_{eu,sep} \propto P_{sep}^{\frac{4}{9}}$, which assumes diffusive radial heat transport, is plotted for each $n_{e,\ sep}$ on Fig. 3 (dashed lines). For lower radiating cases, the scaling captures the variation in $T_{eu,\ sep}$ to a reasonable degree. However, for higher radiating cases, greater than 4 MW for nitrogen and 2 MW for neon the scaling does not capture the variation in $T_{eu,\ sep}$.

### 3.2. Variation in $\boldsymbol{P}_{\boldsymbol{sep}}$ is driven by core impurity radiation

A one-to-one correlation (within 1%) between the input power (into the grid) minus core impurity radiation and $P_{sep}$ was observed (Fig. 4). This implies that the observed variation in $P_{sep}$ is dictated by the amount of impurity radiation occurring inside the separatrix.

Comparing the radiative loss function [4] for a neon and nitrogen simulation with identical $n_{e,\ sep}$ and total impurity radiation, it was found that neon radiates more efficiently inside the separatrix than nitrogen [13]. Hence in all cases where $n_{e,\ sep}$ and the total impurity radiation was the same, neon had a lower $P_{sep}$ than nitrogen.

### 3.3. Variation in $\boldsymbol{q}_{\|,\ \boldsymbol{u,\ sep}}$ is partially driven by main SOL impurity radiation above the x-point

A reduction in $q_{\|,\ u,\ sep}$ was observed when the impurity radiation was present (Fig. 2). For a fixed $n_{e,\ sep}$ an increase in the total impurity radiation leads to a reduction in $q_{\|,\ u,\ sep}$ (Fig. 2). Furthermore, for a comparable simulation, similar $n_{e,\ sep}$ and total impurity radiation, neon seeding causes a larger reduction in $q_{\|,\ u,\ sep}$ than nitrogen compared to an unseeded simulation (Fig. 2).

To confirm that impurity radiation in the main SOL was an important mechanism for the variation in $q_{\|,\ u,\ sep}$, a code study was conducted. The code study removes the impurity radiation from the main SOL (above the $x$-point) only, but still allows for impurity radiation in the divertor (below the $x$-point) and core (inside the separatrix) hence keeping $P_{sep}$ approximately the same. The impurity radiation was set to 2, 4 or 6 MW depending on the simulation chosen minus the contribution of the impurity radiation in the main SOL of that simulation. The radiation was set in this manner to ensure approximately the

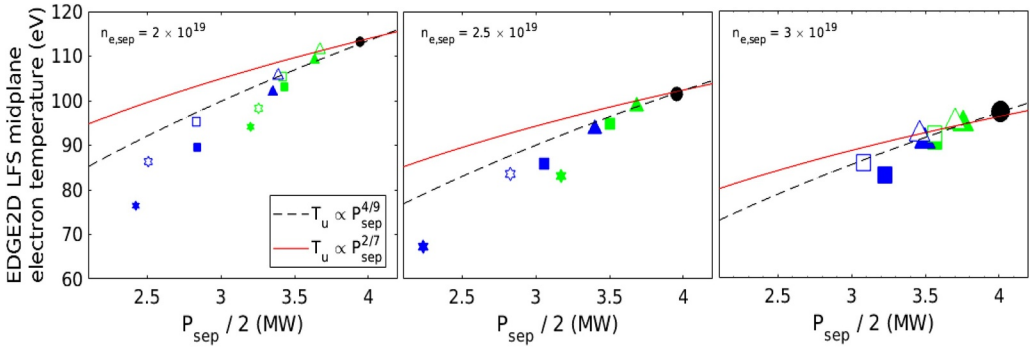


**Fig. 3.** Upstream (LFS) electron temperature from EDGE2D versus power crossing the separatrix divided by 2 (assuming 50% split to HFS and LFS targets). Each plot represents a different separatrix electron density. The markers represent the total seeding radiation: circle – 0 MW (i.e. unseeded); triangle – 2 MW; square – 4 MW; 6-point star – 6 MW. The colour represents the seeding impurity: black – unseeded; green – nitrogen; blue – neon. Increasing size of the symbol represents increasing electron separatrix density ($n_{e,\ sep}$) where the smallest symbol is $n_{e,sep} = 2 \times 10^{19}$ and the largest is $n_{e,sep} = 3 \times 10^{19}$ $m^{-3}$. The open symbols represent the same plasma parameters as the filled markers except within the simulation the impurity radiation has been removed from the scrape-off layer above the *x*-point. The dashed black line represents $T_u = AP_{sep}^{\frac{4}{9}}$ where A was chosen to approximately intersect the unseeded simulation. The solid red line represents $T_u = BP_{sep}^{\frac{2}{7}}$ where B was chosen to approximately intersect the unseeded simulation. (For interpretation of the references to colour in this figure legend, the reader is referred to the web version of this article.)

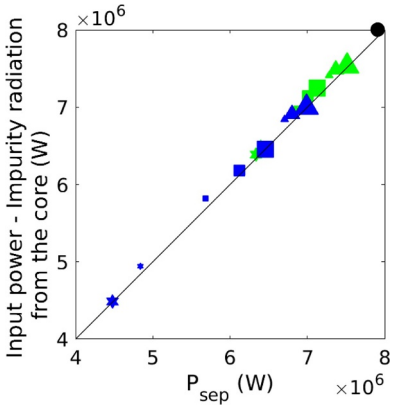


**Fig. 4.** Input power (always 8 MW) to the computational domain minus the total impurity radiation within the separatrix versus the power crossing the separatrix. The markers represent the total seeding radiation: circle – 0 MW (i.e. unseeded); triangle – 2 MW; square – 4 MW; 6-point star – 6 MW. The colour represents the seeding impurity: black – unseeded; green – nitrogen; blue – neon. Increasing size of the symbol represents increasing electron separatrix density ($n_{e,\ sep}$) where the smallest symbol is $n_{e,sep} = 2 \times 10^{19}$ and the largest is $n_{e,sep} = 3 \times 10^{19}$. (For interpretation of the references to colour in this figure legend, the reader is referred to the web version of this article.)

same impurity radiation in the core and divertor regions when seeding radiation was present in the main SOL. The study was run for seeding cases which had an $n_{e,\ sep}$ of $2 \times 10^{19}$, $3 \times 10^{19}$ $m^{-3}$ and 6 MW neon seeded simulation of $n_{e,sep} = 2.5 \times 10^{19}$ $m^{-3}$.

As stated above, for the main simulation set (i.e. impurity radiation present in the main SOL), the $T_{eu,sep} \propto P_{sep}^{\frac{4}{9}}$ does not fully capture the variation in $T_{eu,\ sep}$. This is because there is significant radiation in the near SOL above the *x*-point in the highly radiating simulations, which reduces $q_{\parallel,\ u,\ sep}$. However, the simulations where the radiation was removed in the main SOL show a reduction in $q_{\parallel,\ u,\ sep}$ (open symbols Fig. 2) and follow the $T_{eu,sep} \propto P_{sep}^{\frac{4}{9}}$ scaling more closely (Fig. 3 open symbols and dashed line). The removal of the radiation above the *x*-point causes $T_{eu,\ sep}$ to be driven solely by $P_{sep}$ and by the radial transport which affects $\lambda_q$, both of which are accounted for in the $T_{eu,sep} \propto P_{sep}^{\frac{4}{9}}$ scaling.

### 3.4. Variation in Eich fitted $\lambda_q$ captures the variation in $q_{\parallel,\ u,\ sep}$

The total $q_{\parallel}$ profile at the LFS target was fitted using the Eich fit [14] to calculate $\lambda_{q,\ Eich}$ for each simulation. The choice to use the Eich fit is motivated by the fact that it is experimentally measurable, compared to directly measuring $\lambda_q$ at the divertor entrance, which experimentally is impossible. Note that the 6 MW neon seeded case of $n_{e,sep} = 2.5 \times 10^{19}$ $m^{-3}$ did not have $\lambda_{q,\ Eich}$ calculated because it was detached.

Using $\lambda_{q,\ Eich}$ a value for $A_q$ was calculated (as per Eq. (3)) which from now onwards will be referred to as $A_{q,\ Eich}$. Extracting $P_{sep}$, $L$ and $B_\theta/B$ (note $L$ and $B_\theta/B$ are constant throughout the whole simulation set as the same equilibrium was used) from EDGE2D and using $A_{q,\ Eich}$, an upstream temperature was calculated using Eq. (2). A comparison between this recalculated upstream temperature and the upstream temperature from EDGE2D is shown in Fig. 5. Agreement within approximately 20% of the predicted EDGE2D-EIRENE upstream temperature and the upstream temperature calculated from Eq. (2) was found (Fig. 5). Note that there is, at worst, a systematic underprediction of approximately 20% (Fig. 5) of the upstream temperature calculated from Eq. (2) when compared to EDGE2D. Accounting for the variation in both $\lambda_{q,\ Eich}$ and $P_{sep}$ in each simulation, agreement between Eq. (2) and EDGE2D was yielded.

Eq. (2) agrees with EDGE2D (Fig. 5) because $(P_{sep}/2)/A_{q,\ Eich}$ scales with the variation in $q_{\parallel,\ u,\ sep}$ (Fig. 6). There is a large variation in $A_{q,\ Eich}$

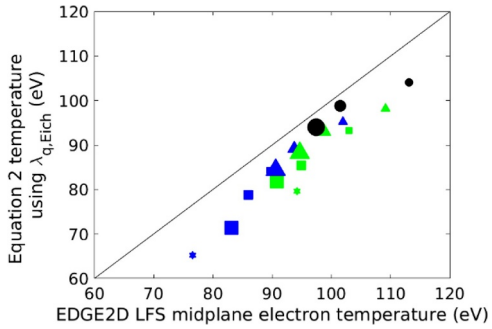


**Fig. 5.** The upstream temperature from EDGE2D-EIRENE compared to the two point model equation [4]. The two point model equation is calculated using the power decay width ($\lambda_q$) from the Eich fit. The markers represent the total seeding radiation: circle – 0 MW; triangle – 2 MW; square – 4 MW; 6-point star – 6 MW. The colour represents the seeding impurity: black – unseeded; green – nitrogen; blue – neon. Increasing size of the symbol represents increasing electron separatrix density ($n_{e,\ sep}$) where the smallest symbol is $n_{e,sep} = 2 \times 10^{19}$ and the largest is $n_{e,sep} = 3 \times 10^{19}$ $m^{-3}$. (For interpretation of the references to colour in this figure legend, the reader is referred to the web version of this article.)

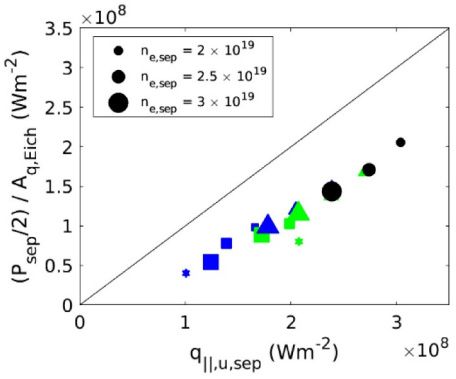


**Fig. 6.** Half of the power crossing the separatrix ($P_{sep}$, assuming 50/50 split of power to the HFS and LFS targets) divided by the area ($A_{q,\ eich}$) which is calculated using Eq. (3) and $\lambda_q$ is taken as value calculated by the Eich fit plotted against $q_{\parallel,\ u,\ sep}$. The markers represent the total seeding radiation: circle – 0 MW; triangle – 2 MW; square – 4 MW; 6-point star – 6 MW. The colour represents the seeding impurity: black – unseeded; green – nitrogen; blue – neon. Increasing size of the symbol represents increasing electron separatrix density ($n_{e,\ sep}$) where the smallest symbol is $n_{e,sep} = 2 \times 10^{19}$ and the largest is $n_{e,sep} = 3 \times 10^{19}\ m^{-3}$. (For interpretation of the references to colour in this figure legend, the reader is referred to the web version of this article.)

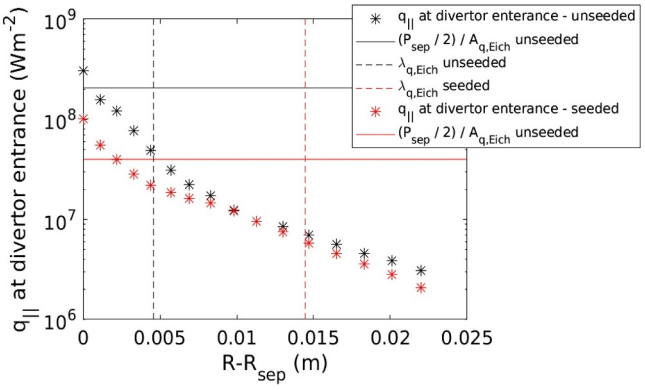


**Fig. 7.** Log plot of the parallel heat flux density profle ($q_{\parallel}$) entering the LFS divertor plotted against LFS midplane coordinate normalised to the separatrix. Black markers represent the $q_{\parallel}$ for an unseeded $n_{e,sep} = 2 \times 10^{19}$ and blue markers the neon seeded $n_{e,sep} = 2 \times 10^{19}$. Horizontal lines represent ($P_{sep}$/2)/$A_q$ where $P_{sep}$ is the power crossing the separatrix and $A_q$ is calculated as per Eq. (3) using $\lambda_q$ calculated from the Eich fit and the colour retains the same meaning as the marker. Solid vertical lines are $\lambda_q$ calculated via the Eich fit and the colour retains the same meaning. (For interpretation of the references to colour in this figure legend, the reader is referred to the web version of this article.)

as $\lambda_{q,\ Eich}$ varies by a factor four over the simulation set (vertical dashed lines Fig. 7). The simultaneous variation of both $P_{sep}$ and $A_{q,\ Eich}$ explains the variation in $T_{eu,\ sep}$ in experimentally measurable variables. However, the reader should note that, no experimental evidence has been found to show that $\lambda_{q,\ Eich}$ or $\lambda_q$ scales with $P_{sep}$.

The Eich fit is used to calculate $\lambda_q$ because it correctly captures the variation in $q_{\parallel,\ u,\ sep}$. The radial variation in the $q_{\parallel}$ profile at the divertor entrance has changed from a typical exponential decay from the separatrix to far SOL (unseeded case - black markers Fig. 7) to an exponential decay that has been clipped off near the separatrix (seeded case - blue markers Fig. 7), but retains the exponential decay shape in the far SOL. This non-exponential decay can be seen on Fig. 7 (blue markers) for around $R - R_{omp} = 0.002 - 0.01\ m$. The reason why the exponential is clipped off is due to the preferential removal of power caused by the impurity radiation above the $x$-point. This change in the radial variation of the $q_{\parallel}$ profile (and $q_{\parallel,\ u,\ sep}$) to a non-exponential decay was captured well by the Eich fit.

## 4. Conclusion

An approximately two-fold increase in upstream temperature ($T_{eu,\ sep}$) was observed within EDGE2D, which is driven by a factor six change in the parallel heat flux entering the divertor at the separatrix ($q_{\parallel,\ u,\ sep}$) thus confirming the scaling $T_{eu,sep} \propto q_{\parallel,u,sep}^{\frac{2}{7}}$. However, only a factor two change in the power crossing the separatrix ($P_{sep}$) was observed. $P_{sep}$ (for constant input power) is exclusively set by the impurity radiation occurring on closed field lines. $P_{sep}$ was lower for neon seeded cases to a comparable nitrogen seeded case because neon radiates more efficiently on closed field lines than nitrogen, hence reducing $P_{sep}$ and thus $T_{eu,\ sep}$. The scaling $T_{eu,sep} \propto P_{sep}^{\frac{4}{9}}$ (which accounts for $\lambda_q$ dependence on $P_{sep}$ and for prescribed diffusive radial transport) captures the variation in the lower seeded simulation but not the higher seeded simulations. Variation in $A_{q,\ Eich}$ (the perpendicular cross-sectional area of the considered flux tube) was strongly affected by the clipping of the near SOL $q_{\parallel}$ profile at the divertor entrance due to impurity radiation above the $x$-point, which renders the profile non-exponential. Nevertheless, our work shows that the Eich fit (which was used to calculate $A_{q,\ Eich}$) can still be used in conjunction with $P_{sep}$ to approximate $q_{\parallel,\ u,\ sep}$. $T_{eu,\ sep}$ was driven by three things: (1) a factor two variation in $P_{sep}$ due to varying core impurity radiation, (2) impurity radiation preferentially removing heat flux above the $x$-point and near the separatrix, and (3) a decrease in $\lambda_q$ with increasing $P_{sep}$ due to a balance of parallel and radial heat flux under the assumption of radially diffusive heat flux [4]. Simulations in which the impurity radiation in the main SOL was removed, the scaling $T_{eu,sep} \propto P_{sep}^{\frac{4}{9}}$ captured the variation $T_{eu,\ sep}$ of these simulations. This is because the scaling $T_{eu,sep} \propto P_{sep}^{\frac{4}{9}}$ accounts for variation in $P_{sep}$ and $\lambda_q$ (assuming that is set by a competition between parallel heat conduction and prescribed diffusive radial heat transport)

Once the variation of $q_{\parallel,\ u,\ sep}$ was accounted for (by using experimentally derived variables $P_{sep}$ and $\lambda_{q,\ Eich}$) an agreement within 20% between EDGE2D-EIRENE upstream temperature and the two point model equation (Eq. (2)) was yielded. A variation of upstream electron temperature from approximately 60–120 eV with seeding, for $n_{e,\ sep}$ range of $2 - 3\ \times 10^{19}\ m^{-3}$, was observed. Hence it is incorrect to assume that the separatrix temperature is invariant due to the weak power scalings shown above. Models that are sensitive to the separatrix temperature should calculate $\lambda_q$ and $P_{sep}$ to predict $T_{eu,\ sep}$ using the two point model equation.

## Acknowledgements

"This work has been carried out within the framework of the EUROfusion Consortium and has received funding from the Euratom research and training programme 2014-2018 under grant agreement no 633053. The views and opinions expressed herein do not necessarily reflect those of the European Commission."

## Supplementary materials

Supplementary material associated with this article can be found, in the online version, at doi:10.1016/j.nme.2019.02.002.

## References

[1] R.J. Goldston, Heuristic drift-based model of the power scrape-off width in low-gas-puff H-mode tokamaks, Nucl. Fusion 52 (2012) 013009, , https://doi.org/10.1088/0029-5515/52/1/013009.
[2] T. Eich, R.J. Goldston, A. Kallenbach, B. Sieglin, H.J. Sun, Correlation of the tokamak H-mode density limit with ballooning stability at the separatrix, Nucl. Fusion 58 (2018) 034001, , https://doi.org/10.1088/1741-4326/aaa340.
[3] H.R. Wilson, P.B. Snyder, G.T. a. Huysmans, R.L. Miller, Numerical studies of edge

localized instabilities in tokamaks, Phys. Plasmas 9 (2002) 1277, https://doi.org/10.1063/1.1459058.
[4] P.C. Stangeby, The Plasma Boundary of Magnetic Fusion Devices, (2000).
[5] S. Saarelma, A. Järvinen, M. Beurskens, C. Challis, L. Frassinetti, C. Giroud, M. Groth, M. Leyland, C. Maggi, J. Simpson, The effects of impurities and core pressure on pedestal stability in Joint European Torus (JET), Phys. Plasmas (2015) 22, https://doi.org/10.1063/1.4921413.
[6] A.E. Jaervinen, M. Groth, M. Airila, P. Belo, M. Beurskens, S. Brezinsek, M. Clever, G. Corrigan, S. Devaux, P. Drewelow, T. Eich, C. Giroud, D. Harting, A. Huber, S. Jachmich, K. Lawson, B. Lipschultz, G. Maddison, C. Maggi, T. Makkonen, C. Marchetto, S. Marsen, G.F. Matthews, A.G. Meigs, D. Moulton, M.F. Stamp, S. Wiesen, M. Wischmeier, Interpretation of radiative divertor studies with impurity seeding in type-I ELMy H-mode plasmas in JET-ILW using EDGE2D-EIRENE, J. Nucl. Mater. 463 (2015) 135–142, https://doi.org/10.1016/j.jnucmat.2014.10.047.
[7] A.E. Jaervinen, S. Brezinsek, C. Giroud, M. Groth, C. Guillemaut, P. Belo, M. Brix, G. Corrigan, P. Drewelow, D. Harting, A. Huber, K.D. Lawson, B. Lipschultz, C.F. Maggi, G.F. Matthews, A.G. Meigs, D. Moulton, M.F. Stamp, S. Wiesen, Impact of divertor geometry on radiative divertor performance in JET H-mode plasmas, Plasma Phys. Control. Fusion 58 (2016) 45011, https://doi.org/10.1088/0741-3335/58/4/045011.
[8] R. Simonini, G. Corrigan, G. Radford, J. Spence, A. Taroni, Models and numerics in the multi-fluid 2-D edge plasma code EDGE2D/U, Contrib. Plasma Phys. 34 (1994) 368–373, https://doi.org/10.1002/ctpp.2150340242.
[9] S. Wiesen, ITC Report, (2006) www.eirene.de/e2deir_ report_30jun06.pdf.
[10] D. Reiter, C. May, D. Coster, R. Schneider, Time dependent neutral gas transport in tokamak edge plasmas, J. Nucl. Mater. 220–222 (1995) 987–992, https://doi.org/10.1016/0022-3115(94)00648-2.
[11] C. Giroud, G.P. Maddison, S. Jachmich, F. Rimini, M.N.A. Beurskens, I. Balboa, S. Brezinsek, R. Coelho, J.W. Coenen, L. Frassinetti, E. Joffrin, M. Oberkofler, M. Lehnen, Y. Liu, S. Marsen, K. McCormick, A. Meigs, R. Neu, B. Sieglin, G. Van Rooij, G. Arnoux, P. Belo, M. Brix, M. Clever, I. Coffey, S. Devaux, D. Douai, T. Eich, J. Flanagan, S. Grünhagen, A. Huber, M. Kempenaars, U. Kruezi, K. Lawson, P. Lomas, C. Lowry, I. Nunes, A. Sirinnelli, A.C.C. Sips, M. Stamp, S. Wiesen, Impact of nitrogen seeding on confinement and power load control of a high-triangularity JET ELMy H-mode plasma with a metal wall, Nucl. Fusion (2013) 53, https://doi.org/10.1088/0029-5515/53/11/113025.
[12] D.J. Moulton, Numerical Modelling of H-mode Plasmas on JET, PhD Thesis (2012).
[13] A. Järvinen, Radiative Divertor Studies in JET High Confinement Mode Plasmas, PhD Thesis (2015).
[14] T. Eich, B. Sieglin, A. Scarabosio, W. Fundamenski, R.J. Goldston, A. Herrmann, Inter-ELM power decay length for JET and ASDEX Upgrade: measurement and comparison with heuristic drift-based model, Phys. Rev. Lett. 107 (1–4) (2011), https://doi.org/10.1103/PhysRevLett.107.215001.